PHYSICAL REVIEW D **76,** 125030 (2007)

Cosmogenic neutrinos and quasistable supersymmetric particle production

M. H. Reno
Department of Physics and Astronomy, University of Iowa, Iowa City, Iowa 52242, USA

I. Sarcevic and J. Uscinski
Department of Physics, University of Arizona, Tucson, Arizona 85721, USA
(Received 29 October 2007; published 27 December 2007)

We study the signal for the detection of quasistable supersymmetric particle produced in interactions of cosmogenic neutrinos. We consider energy loss of high-energy staus due to photonuclear and weak interactions. We show that there are optimal nadir angles for which the stau signal is a factor of several hundred larger than muons. We discuss how one could potentially eliminate muon background by considering the energy loss of muons in the detector. We also show results for the showers produced by weak interactions of staus that reach the detector.

DOI: 10.1103/PhysRevD.76.125030 PACS numbers: 14.80.Ly

I. INTRODUCTION

Ultrahigh energy (UHE) cosmic neutrinos could potentially probe physics beyond the standard model [1]. Interactions of UHE neutrinos ($E_\nu \geq 10^{17}$ eV) with nucleons probe center of mass energies above 14 TeV. Some fraction of these neutrinos may produce supersymmetric particles or some other exotic particles. These processes are suppressed relative to standard model processes; however, in some models interesting signals may arise from supersymmetric particles with long lifetimes. In most supersymmetry (SUSY) scenarios, particles produced in high-energy collisions decay immediately into the lightest one and are thus hard to detect. However in some low-scale supersymmetric models in which gravitino is the lightest supersymmetric particle (LSP) and R-parity is conserved, the next-to-lightest particle (NLSP) is the charged superpartner of the right-handed tau, the stau [2]. Because of its weak coupling to the gravitino, the stau is a long-lived particle in these models. For the supersymmetric breaking scale, $\sqrt{F} > 5 \times 10^6$ GeV, the long-lived stau could travel distances of the order of 10^4 km before decaying into the gravitino.

The distance that staus travel before decaying depends on the gravitino mass (or equivalently on the supersymmetry breaking scale) and the stau mass. Limits on the stau mass of about 100 GeV come from its nonobservation in accelerator experiments [3–6]. Recently it was proposed that staus produced in high-energy neutrino interactions, where neutrinos originate in astrophysical sources, might be detectable in neutrino telescopes [7,8].

The cross section for the production of staus in neutrino-nucleon scattering [7] is several orders of magnitude smaller than the neutrino charged-current or neutral-current cross section [9]. However, once produced, the long-lived staus have the potential to travel through the Earth without decaying and thus open up a possibility to be detected in neutrino telescopes. The long range of staus could potentially compensate for the suppression in the production cross section by increasing the effective detector volume and therefore enhancing the signal.

The detection of staus depends on the stau lifetime and range, so it is important to determine the energy loss as it traverses the Earth. The details of the range depend in part on the supersymmetry breaking and how the quasistable stau particle is composed of the SUSY partners of the right-handed and left-handed taus. The electromagnetic energy loss has been shown to have the largest contribution from photonuclear interactions for stau energies between 10^6–10^{12} GeV, resulting in a range of 10^4 km w.e. for masses of the order of a few hundred GeV [10]. Weak interactions may come into play as well. The stau range has been shown to be sensitive to the mixing angle of right-handed and left-handed staus. When the mixing is maximal, weak interactions act to suppress the range at energies above $\sim 10^9$ GeV [11]; however, their weak interactions have the potential to produce signals in neutrino detectors such as the Antarctic Impulse Transient Array (ANITA) [12] and the Antarctic Ross Iceshelf Antenna Neutrino Array (ARIANNA) [13].

The high energies required for stau production lead us to focus on the production of staus in interactions of cosmogenic neutrinos as they traverse the Earth and/or in the detector. These neutrinos originate from cosmic ray protons interacting with the cosmic microwave background,

$$p\gamma(3\mathrm{K}) \rightarrow \Delta \rightarrow N\pi,$$

followed by charged pion, muon and neutron decays. This flux is guaranteed as cosmic ray fluxes are measured as well as the 3K microwave background. We use a conservative cosmogenic neutrino flux evaluated by Engel, Seckel and Stanev (ESS) in Ref. [14]. They evaluate the neutrino flux associated with the measured cosmic ray flux by tracing back cosmic ray propagation through the background radiation. Depending on the cosmological evolution assumed, the overall normalization of this flux has an uncertainty of about a factor of 4. In addition, neutrinos

could be produced at the sources of the high-energy cosmic rays, and those are not included in the evaluation of ESS neutrino flux. Thus, the ESS neutrino flux is a conservative estimate of the cosmogenic flux.

The cosmogenic neutrino flux, when neutrino flavor oscillations are not included, peaks at high energies, around 10^8 GeV, and thus it is in the energy range where ANITA and ARIANNA have very good sensitivity [12,13]. The neutrino flavor ratio for cosmogenic neutrinos deviates from the common 2:1 ratio, due to the neutron decay contribution to electron neutrinos [14]. This implies that one needs to consider three flavor oscillations when considering the cosomogenic neutrino flux that arrives at the Earth [15].

We consider cosmogenic neutrinos, their propagation, stau production, and subsequent energy loss as it traverses the Earth, for a region of parameter space where the staus do not decay over the distances required. We compare the resulting stau flux when there is no mixing between right-handed and left-handed stau and when there is maximal mixing. We consider muonlike signals (charged tracks) produced by staus and their associated background. We discuss the potential for eliminating the background by measuring the energy loss, which requires large volume detectors. Finally we discuss the showers produced in the ice due to stau interactions and its background from neutrino-induced showers.

II. CHARACTERISTIC DISTANCE SCALES AND STAU PRODUCTION

The potential for staus to have a long lifetime is an essential feature of this analysis. The lifetime of the stau depends on the supersymmetry breaking scale ($F^{1/2}$) and stau mass ($m_{\tilde{\tau}}$). It is given by

$$c\tau = \left(\frac{F}{10^{14}\ \mathrm{GeV}^2}\right)^2 \left(\frac{100\ \mathrm{GeV}}{m_{\tilde{\tau}}}\right)^5 10\ \mathrm{km}. \qquad (1)$$

In Fig. 1, we show the parameter space ($m_{\tilde{\tau}}$, $\sqrt{F}$) and the region for which staus with certain energy (10^8, 10^{10}, 10^{12} GeV) have long-enough lifetimes, $\gamma c\tau = 10^7$ cm w.e., to travel through the Earth without decaying for a nadir angle of 88°. Different nadir angles, or column depths, correspond to different ranges of these parameters. Clearly there is a large parameter space in which staus do not decay, but they may interact via charged-current interactions, if there is a maximal mixing between the right-handed and left-handed stau. Here we consider the case when stau mass is 150 GeV and the supersymmetric breaking scale $F^{1/2} = 10^7$ GeV.

Staus are produced in neutrino-nucleon interactions in the Earth with the cross sections [7] about 3 orders of magnitude smaller than standard model neutrino weak interactions with nucleons [9]. The staus are produced by the decays of heavy quarks and sleptons produced in the primary neutrino-nucleon interactions. The cross section

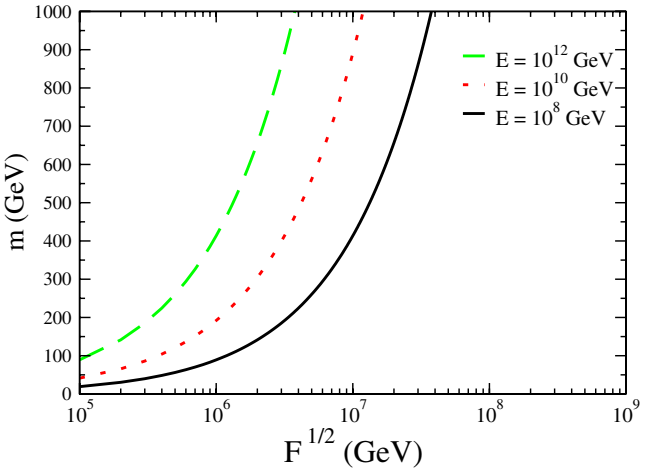

FIG. 1 (color online). The parameter space of stau mass m and decay parameter $F^{1/2}$ probed with stau decay lengths corresponding to a column depth of 10^7 cm w.e. The area to the right of each curve is the parameter space probed by demanding that stau does not decay as it traverses this column depth.

for the stau production is a t-channel production of a slepton and a squark via gaugino exchange. This cross section depends on the squark mass, gaugino masses and the mass of the left-handed slepton. We take the cross section for stau production obtained with $m_{\tilde{q}} = 300$ GeV, $m_{\tilde{w}} = 250$ GeV and $m_{\tilde{l}_L} = 250$ GeV [7]. Stau cross sections obtained using different parameters and different SUSY models are shown in Ref. [8]. The cross section converted into an interaction length,

$$\mathcal{L} = (N_A \sigma)^{-1}, \qquad (2)$$

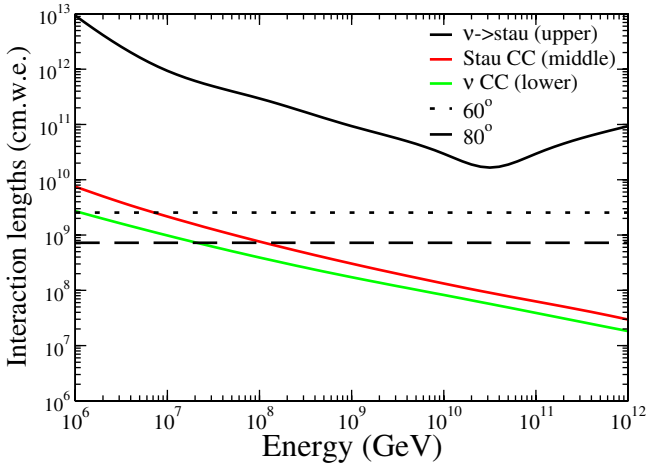

FIG. 2 (color online). Interaction lengths for neutrinos and staus. The solid curves, from top to bottom, are the interaction lengths for neutrinos to produce staus, for stau charged-current interactions with maximal weak interactions, and for neutrino CC interactions. The dotted and dashed lines show the column depths for nadir angles of 60° and 80°.

is shown for neutrino production of staus by the upper solid line in Fig. 2.

Cosmic neutrino fluxes that reach the Earth get attenuated as neutrinos traverse the Earth toward the detector, due to weak interactions, primarily the charged-current (CC) interactions. Similarly, once created in neutrino-nucleon interactions, the stau flux also gets attenuated when staus interact weakly. The size of these effects can be seen in Fig. 2, where we show neutrino interaction length [9] and the stau interaction length [11] due to their charged-current interactions with isoscalar nucleons, as a function of incident energy. This figure shows the stau charged-current cross section with maximal weak interactions. We also show for reference the column depth for nadir angles of 60° and 80°.

III. LEPTON AND STAU FLUXES

A. Cosmogenic flux

The cosmogenic fluxes that we use as reference input fluxes are the standard evolution and strong evolution fluxes of Engel, Seckel and Stanev [14]. The fluxes are of neutrinos and antineutrinos, with an electron neutrino to muon neutrino flavor ratio that depends on energy. Part of this energy dependence comes from the eventual neutron decay in $p\gamma \rightarrow n\pi^+$ production.

Neutrino oscillations due to nonzero neutrino masses modify the neutrino flavor ratio over the cosmological distances they travel. Consequently, we use for the cosmogenic fluxes at the Earth [15],

$$F_{\nu_e} = F^0_{\nu_e} - \tfrac{1}{4}\sin^2 2\theta_{12}(2F^0_{\nu_e} - F^0_{\nu_\mu} - F^0_{\nu_\tau}) \qquad (3)$$

$$F_{\nu_\mu} = F_{\nu_\tau} = \tfrac{1}{2}(F^0_{\nu_\mu} + F^0_{\nu_\tau}) + \tfrac{1}{8}\sin^2 2\theta_{12}(2F^0_{\nu_e} - F^0_{\nu_\mu} - F^0_{\nu_\tau}), \qquad (4)$$

where F^0_i are the ESS cosmogenic fluxes [14]. The cosmogenic tau neutrino flux $F^0_{\nu_\tau} = 0$ because of the threshold for tau production: the dominant process of resonant Δ production ultimately results in only ν_e and ν_μ fluxes at the point of production. The expressions in Eqs. (3) and (4) are written with the assumption of maximal mixing between ν_μ and ν_τ. For the numerical work below, we have taken $\theta_{12} = 33°$.

In Fig. 3, the total neutrino plus antineutrino cosmogenic fluxes are shown with the upper (strong evolution) and lower (standard evolution) solid lines. Without neutrino oscillations, the corresponding $\nu_\mu + \bar{\nu}_\mu$ fluxes are shown by the dashed lines. Including neutrino oscillations, the $\nu_\mu + \bar{\nu}_\mu$ cosmogenic strong and standard evolution fluxes are shown by the dot-dashed lines. Neutrino oscillations enhance the incident muon (anti)neutrino flux at low energies due to $\bar{\nu}_e \rightarrow \bar{\nu}_\mu$ oscillations.

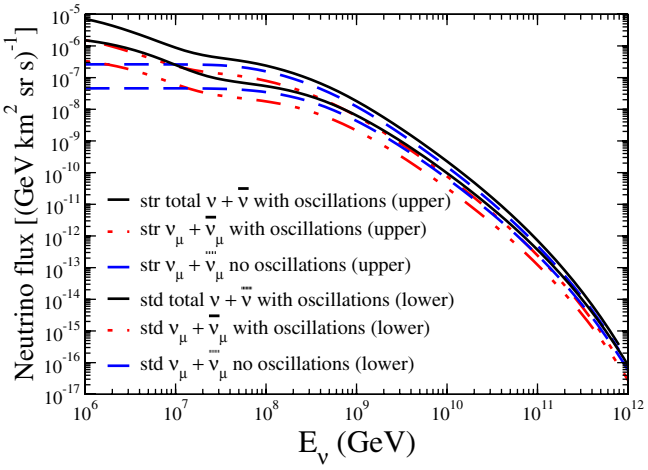

FIG. 3 (color online). Cosmogenic neutrino flux with standard evolution and with strong evolution [14]. The upper (lower) solid lines represent the total neutrino plus antineutrino flux for strong (standard) evolution, dashed lines are the $\nu_\mu + \bar{\nu}_\mu$ flux without including oscillation effects, and the dot-dashed lines represent $\nu_\mu + \bar{\nu}_\mu$ flux with oscillation effects included.

Finally, as noted above, the cosmogenic neutrino fluxes shown in Fig. 3 are considered "conservative." They correspond to neutrinos produced by cosmic rays interacting with the 3K radiation. Neutrinos could also be produced in some cosmic accelerators, such as active galactic nuclei and gamma ray bursts, but the fluxes have large theoretical uncertainties [16]. The cosmogenic neutrino flux calculations have a number of uncertainties including the effect of cosmogenic evolution. Nevertheless we focus on the cosmogenic neutrinos from cosmic ray interactions with the microwave background because they are a "guaranteed" source of ultrahigh energy neutrinos.

B. Muon flux

Muons are produced by $\nu_\mu N$ charged-current interactions. Electromagnetic energy loss of muons passing through matter together with a survival probability that depends on lifetime and energy determine the muon flux. Electromagnetic energy loss is described by the average change in energy per unit column depth $X = \rho z$ (in terms of density ρ and distance z) via

$$\frac{dE}{dX} = -(\alpha + \beta_\mu E). \qquad (5)$$

The radiative energy loss due to bremsstrahlung, pair production and photonuclear scattering, characterized by β_μ, increases with energy from about $\simeq 4 \times 10^{-6}$ cm^2/g for $E_\mu \sim 10^3$ GeV to about $\simeq 5$–6×10^{-6} cm^2/g for $E_\mu \sim 10^9$ GeV [17]. Here we take $\beta_\mu \simeq 4 \times 10^{-6}$ cm^2/g, which will correspond to the maximum background for the stau charged-track signal due to muons. With $\alpha \simeq 2 \times 10^{-3}$ GeV cm^2/g [18], for the energies con-

sidered here, $dE/dX \simeq -\beta_\mu E$. Equation (5) combined with effects of the finite muon lifetime on the survival probability $P_{\rm surv}$,

$$\frac{dP_{\rm surv}}{dX} = -\frac{P_{\rm surv}}{c\tau\rho E/m} \tag{6}$$

leads to

$$P_{\rm surv} = \exp\left[-\frac{m_\mu}{c\tau_\mu\beta_\mu\rho}\left(\frac{1}{E_\mu} - \frac{e^{-\beta_\mu(L-X)}}{E_\mu}\right)\right]. \tag{7}$$

The muon flux produced by incident muon neutrinos, for column depth L, is given by

$$F_\mu(E_\mu, L) \simeq \int_0^L dX \int dE_\nu e^{-X\sigma_{CC}(E_\nu)N_A} F_{\nu_\mu}(E_\nu, 0) \times N_A\sigma_{\nu\to\mu}(E_\nu)\delta(E_\mu - 0.8E_\nu e^{-\beta_\mu(L-X)}) \times \exp\left[-\frac{m_\mu}{c\tau_\mu\beta_\mu\rho}\left(\frac{1}{E_\mu} - \frac{e^{-\beta_\mu(L-X)}}{E_\mu}\right)\right], \tag{8}$$

where we have made some simplifying approximations. We have approximated the neutrino-nucleon charged-current differential cross section by

$$\frac{d\sigma_{\nu\to\mu}(E_\nu, E'_\mu)}{dE'_\mu} \simeq \sigma_{\nu\to\mu}(E_\nu)\delta(E'_\mu - 0.8E_\nu)$$

where E'_μ is the energy of the produced muon. This is the energy of the muon before it loses energy via electromagnetic interactions. The flux F_ν represents the $\nu_\mu + \bar\nu_\mu$ flux, and F_μ is the sum of muon and antimuon fluxes.

We have also approximated the attenuation of the neutrino flux in transit through a column depth X by the shadow factor

$$S \equiv \exp(-\sigma^{\nu N}_{\rm CC}(E_\nu)N_A X). \tag{9}$$

The muon fluxes, as a function of muon energy, are shown in Figs. 4 and 5 with dotted lines for two nadir angles, 80° and 88°. Also shown on these figures are the stau fluxes, to which we now turn.

C. Stau fluxes

The stau flux depends on a number of inputs. We use the squark and slepton masses indicated in Sec. II yielding the $\nu \to \tilde\tau$ interaction length shown in Fig. 2. A further choice of parameter is the mixing angle between weak isospin zero and weak isospin 1/2 scalars, the right-handed and left-handed staus, that yields the mass eigenstate of the NLSP stau. We consider two limiting cases: staus with no weak interactions, and staus with maximal weak interactions [11].

We start with the case of no weak interactions. In this case, the evaluation of the stau flux is similar to that of the muon flux. In Ref. [10], we showed that for staus, a reasonable parametrization of the energy loss parameter $\beta_{\tilde\tau}$ is

$$\beta_{\tilde\tau} = b_0 + b_1 \ln(E/E_0), \qquad b_0 = 5\times10^{-9}\ {\rm cm^2/g},$$
$$b_1 = 2.8\times10^{-10}\ {\rm cm^2/g}, \qquad E_0 = 10^{10}\ {\rm GeV}. \tag{10}$$

With the expression in Eq. (10), the stau survival probability and the relation between the initial stau energy and the final stau energy as a function of distance is modified from the constant β case, namely [19]

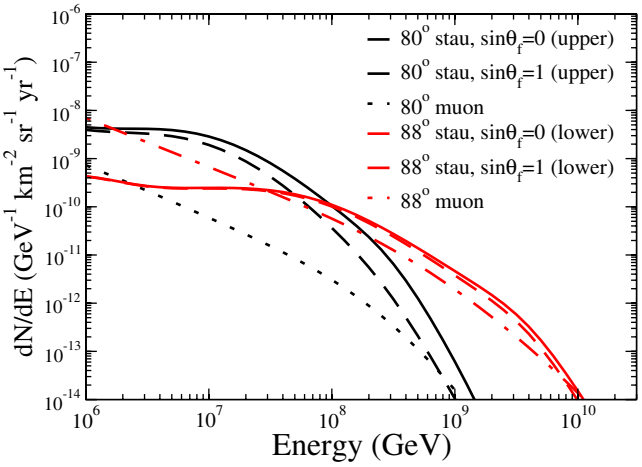

FIG. 4 (color online). For fixed nadir angles of 80° and 88°, the stau flux assuming no weak interactions of the staus (solid lines) and assuming maximal weak interactions (dashed lines) produced by the ESS neutrino flux with standard evolution, evaluated using Eq. (13) and an input flux with including oscillations. The dotted line shows the neutrino-induced muon flux at 80°.

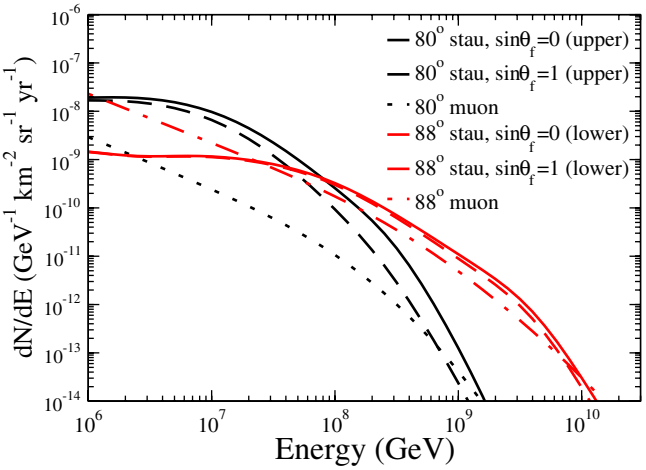

FIG. 5 (color online). For fixed nadir angles of 80° and 88°, the stau flux assuming no weak interactions of the staus (solid lines) and maximal weak interactions (dashed lines) produced by the ESS neutrino flux with strong evolution, evaluated using Eq. (13) and an input neutrino flux with oscillations. The dotted line shows the neutrino-induced muon flux at 80°.

$$E^i_{\tilde\tau}(E_{\tilde\tau}) = E_0 \exp\left[\left[\frac{b_0}{b_1}(1 - e^{-b_1(L-X)}) + \ln\frac{E_{\tilde\tau}}{E_0}\right]e^{b_1(L-X)}\right] \tag{11}$$

$$P_{\rm surv}(E_{\tilde\tau}, E^i_{\tilde\tau}) = \exp\left(\frac{m_{\tilde\tau} b_1}{c\tau\rho b_0^2}\left[\frac{1}{E_{\tilde\tau}}(1 + \ln(E_{\tilde\tau}/E_0) - \frac{1}{E^i_{\tilde\tau}}(1 + \ln(E^i_{\tilde\tau}/E_0)\right]\right) \times \exp\left[-\frac{m_{\tilde\tau}}{c\tau b_0\rho}\left(\frac{1}{E_{\tilde\tau}} - \frac{1}{E^i_{\tilde\tau}}\right)\right]. \tag{12}$$

This leads to a stau flux of

$$F_{\tilde\tau}(E_{\tilde\tau}, L) \simeq 2\int_0^L dX \int dE_\nu e^{-X\sigma_{CC}(E_\nu)N_A} F_\nu(E_\nu, 0) \times N_A\sigma_{\nu\to\tilde\tau}(E_\nu)\delta\left(E_{\tilde\tau} - \frac{1}{6}E_\nu\frac{E_{\tilde\tau}}{E^i_{\tilde\tau}(E_{\tilde\tau})}\right) \times P_{\rm surv}(E_{\tilde\tau}, E^i_{\tilde\tau}). \tag{13}$$

The prefactor of 2 accounts for the fact that the staus appear in pairs, one from each of the chain of decays of the initial squark and slepton. All of the neutrino plus antineutrino flavors are included in $F_\nu(E_\nu, 0)$.

When weak interactions are included, there is an effect due to the attenuation of the staus themselves. The survival probability is modified and is given by

$$\frac{dP_{\rm surv}}{dX} = -\frac{P_{\rm surv}}{\lambda_{\rm eff}} \tag{14}$$

$$\lambda^{-1}_{\rm eff} = (c\tau\rho E/m_{\tilde\tau})^{-1} + N_A\sigma^{CC}(\tilde\tau N). \tag{15}$$

The solution of the combined equations Eqs. (5) and (14) is done numerically.

The resulting stau fluxes for fixed nadir angles of 80°, 85° and 88° are shown as a function of stau energy in Fig. 4 for the ESS standard evolution flux, and in Fig. 5 for the strong evolution. In these figures, the solid lines are for minimal weak interactions, while the dashed lines are for maximal weak interactions.

IV. STAU SIGNALS

A. Stau charged tracks

The fluxes of staus and muons depend on the initial neutrino fluxes, the production cross sections, and the energy loss parameter β. As noted in Sec. III, for the stau signal, the initial neutrino flux includes all neutrino flavors while for muons, only the oscillated $\nu_\mu + \bar\nu_\mu$ flux contributes. The neutrino energy required to produce a stau or a muon of comparable initial energy along the trajectory through the Earth is about 5 times higher for the stau because the mean energy of the resulting stau is approximately 1/6 of the incident neutrino energy, in contrast to the muon case where $E'_\mu \sim 0.8E_\nu$. This means we are probing higher energy neutrinos for staus than for muons to produce a quasistable particle of a given energy. On the other hand, the muons lose more energy in transit from the production point to the detection point.

The production cross section for staus is approximately 3 orders of magnitude smaller than the muon production cross section. Once the staus are produced, they lose very little energy as they traverse the Earth while the muon energy loss is of the order 10^2–10^3 times greater. The stau range can be as high as 10^4 km w.e. for vanishing charged-current interactions or suppressed to about 10^3 km w.e. for maximal charged-current interactions, both higher than the muon range. The neutrino attenuation will also have a large effect on the signals. This attenuation acts to deplete more muons than staus since the muons must be created very near the detector to be seen, whereas the staus can be produced farther away.

These competing effects account for the large stau/muon ratio for specific angles and particle energies. In Fig. 6, we show the ratio of the stau flux to the muon flux for the angles 80°, 85° and 88°, as a function of energy, for standard ESS evolution. The solid lines show the ratio in the scenario where stau weak interactions do not occur. The effect of including maximal charged-current interactions of the staus can be seen by the suppression in the ratio, shown with the dashed lines. We note that the suppression in the ratio begins to take effect between 10^6 and 10^7 GeV, where the stau range begins to be affected by stau charged-current interactions [11]. In Fig. 6, the largest ratio occurs for the nadir angle of 80° which represents the largest path length through the Earth of the trajectories shown. As the nadir angle is decreased, there is an enhancement in the ratio until it reaches a maximum value, and then it drops off when the neutrino attenuation begins to be the dominant

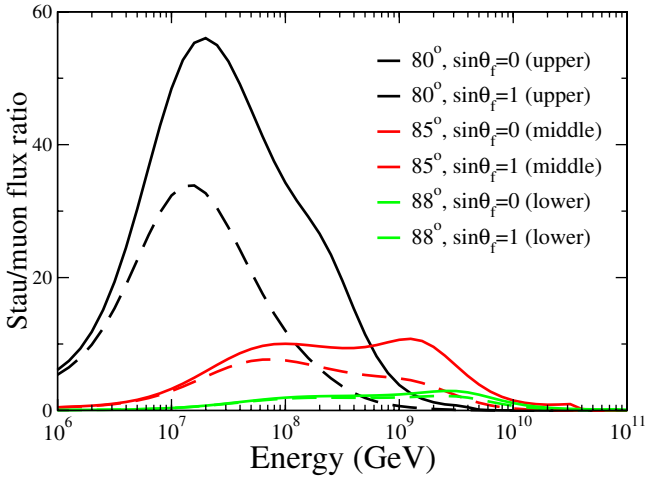

FIG. 6 (color online). For fixed nadir angles of 80°, 85° and 88°, the ratio of the stau flux assuming no weak interactions of the staus (solid lines) and maximal weak interactions (dashed lines) to the muon flux produced by the ESS neutrino flux with standard evolution, including oscillations.

effect for the signal. At lower energies, $E_{\tilde{\tau}} \sim 2 \times 10^6$ GeV, the maximum ratio is 125 (at 70°) when stau maximum weak interactions are included and it is 280 when there are no stau weak interactions. Furthermore, our signal-to-background ratios increase by about 50% (for energy around 10^7 GeV) if we incorporate energy-dependent muon energy loss, by increasing β_μ value to $\beta_\mu \simeq 6 \times 10^{-6}$ cm^2/g.

Figure 7 shows the same effects for strong ESS evolution where the ratio is somewhat reduced. We show in Figs. 8 and 9 the ratio for stau/muon fluxes as a function of angle for the two fixed final particle energies 10^7 and 10^8 GeV, for ESS standard and strong evolutions. Again, we see the same enhancement of stau/muon ratio shifted to the lower angles shown. The strong ESS evolution shows the same behavior as standard evolution, again with a suppressed ratio.

Figures. 6–9 show a significant enhancement of the stau flux relative to the muon flux for various energies and angles. Extracting the stau signal, however, is quite difficult. At issue is the fact that apart from stau decays and charged-current interactions, the stau moves through matter in a way similar to a lower energy muon: the stau signal is muonlike.

In terms of electromagnetic energy loss, one of the issues is that the average of the energy loss per unit distance at high energy scales with βE. The electromagnetic energy loss parameter β for pair production and photonuclear contributions to the energy loss scales as the inverse mass of the charged particle. The bremsstrahlung process, important for muon energy loss, is negligible for stau energy loss since it scales with the inverse mass squared.

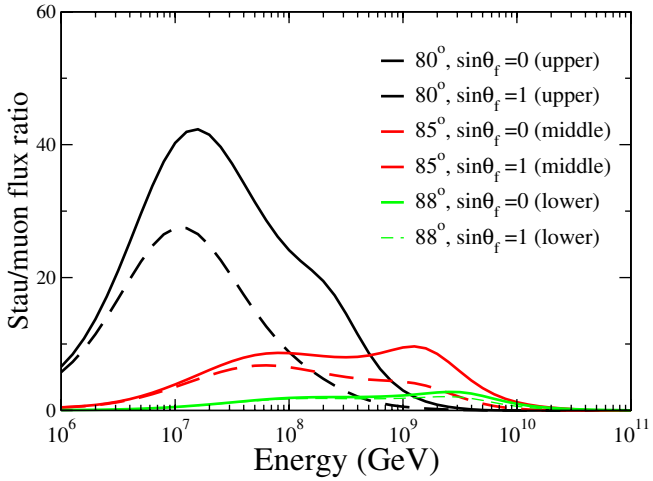

FIG. 7 (color online). For fixed nadir angles of 80°, 85° and 88°, the ratio of the stau flux assuming no weak interactions of the staus (solid lines) and maximal weak interactions (dashed lines) to the muon flux produced by the ESS neutrino flux with strong evolution, including neutrino oscillations.

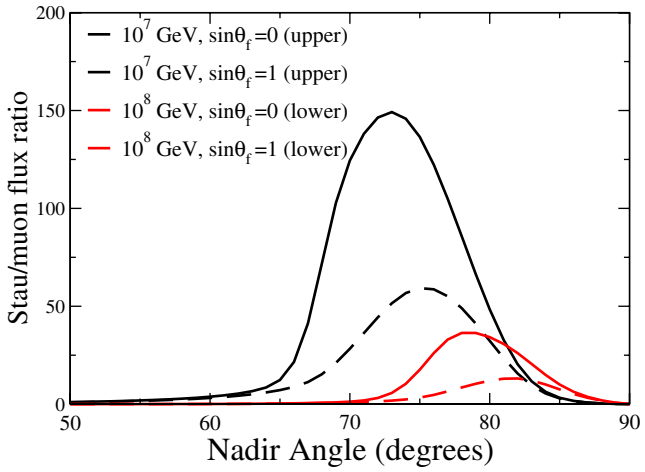

FIG. 8 (color online). For fixed energies of 10^7 and 10^8 GeV, the ratio of the stau flux assuming no weak interactions of the staus (solid lines) and maximal weak interactions (dashed lines) to the muon flux produced by the ESS neutrino flux with standard evolution, including oscillations.

An important element of the energy loss is the electron positron pair production cross section. This cross section is important at low values of the inelasticity parameter v where

$$v = \frac{E - E'}{E}, \tag{16}$$

the ratio of the change in muon or stau energy to the initial energy. In Fig. 10 we show the differential cross section $v d\sigma/dv$ scaled by N_A/A for muons scattering in iron [20,21]. For ease of viewing the small v region, we plot the differential cross section versus $1/v$. Because the pho-

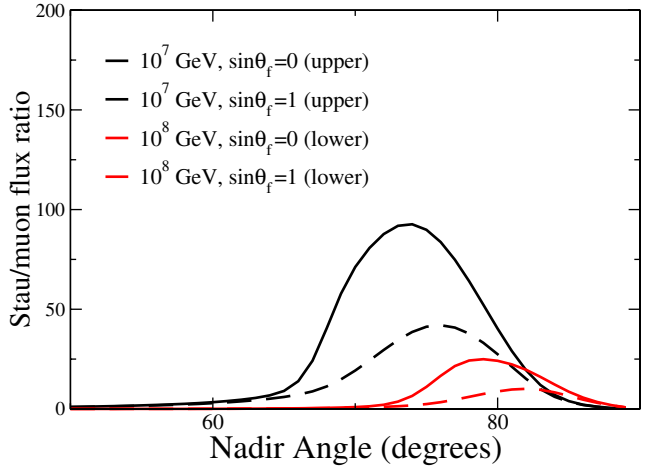

FIG. 9 (color online). For fixed energies of 10^7 and 10^8 GeV, the ratio of the stau flux assuming no weak interactions of the staus (solid lines) and maximal weak interactions (dashed lines) to the muon flux produced by the ESS neutrino flux with strong evolution, including neutrino oscillations.

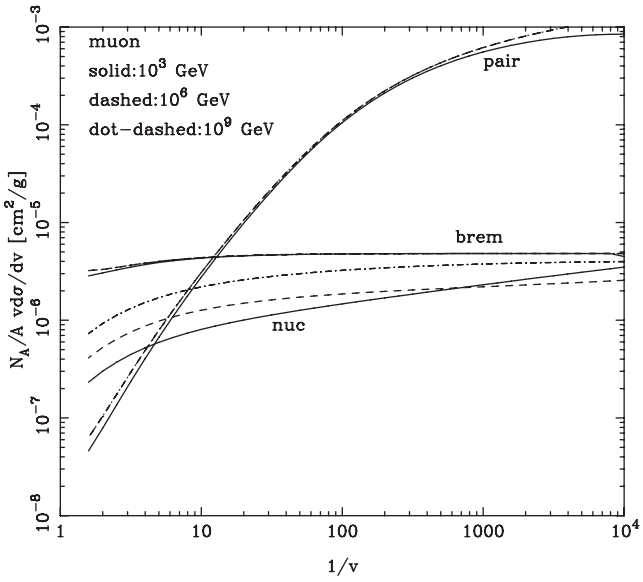

FIG. 10. The inelasticity weighted differential cross section for muons for three muon energies: 10^3 GeV (solid lines), 10^6 GeV (dashed lines) and 10^9 GeV (dot-dashed lines) for pair production, bremsstrahlung and photonuclear energy loss processes.

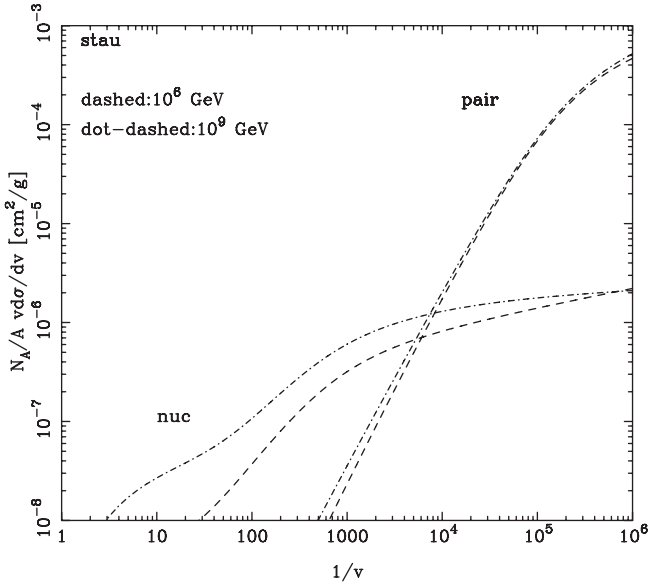

FIG. 11. The inelasticity weighted differential cross section for staus for two stau energies: 10^6 GeV (dashed lines) and 10^9 GeV (dot-dashed lines) for pair production and photonuclear energy loss processes. Bremsstrahlung energy losses are negligible for staus.

tonuclear process includes inelastic scattering corrections [17,22], the differential cross section depends on the incident muon energy. Pair production dominates for $1/v$ greater than $\sim$10, that is to say for muon energy losses of less than $\sim$10% of the initial muon energy.

The corresponding differential cross section for staus is shown in Fig. 11. This figure shows that the dominant process for energy loss of staus is pair production only for energy losses of less than $v \sim 10^{-4}$. Similar results are obtained for ice.

Figures 10 and 11 can be interpreted in terms of the average energy loss $\langle dE/dX \rangle$. For a stau of energy $E_{\tilde{\tau}}$, the average energy loss per unit distance is of order of that of a muon with energy $E_\mu \sim 10^{-3} E_{\tilde{\tau}} \sim m_\mu/m_{\tilde{\tau}} \cdot E_{\tilde{\tau}}$. If the average energy loss per unit distance is the only observable quantity, the large stau to muon ratios are unobservable because one must compare the high-energy stau flux with the lower energy, but significantly larger, muon flux. Quantitatively, this is shown in Fig. 12. Here we take the ratio of the stau flux at energy $E_{\tilde{\tau}} = m_{\tilde{\tau}}/m_\mu \cdot E_\mu$ to the muon flux evaluated at E_μ. We note that the ratio is peaked at the same angle as in Fig. 8, but the ratio is much smaller. This is because $\langle dE/dX \rangle$ matches, for example, muons with energies of 10^7 GeV to staus with energies more than 2 orders of magnitude higher, where the stau flux is low.

The v-dependence of the cross sections in Figs. 10 and 11 may open a window for differentiating muons and staus in the future. Figure 11 shows a marked difference between muons and staus for large v (small $1/v$). An energy deposit of 10% of the initial stau energy of $E_{\tilde{\tau}} = 10^8$ GeV is observed in a stau signal interaction, with very little in the way of comparable energy losses nearby since the large v cross section is so low. With such a large energy loss (say, $\Delta E = 0.1 E_{\tilde{\tau}}$), there would be no confusing the stau with muon with an energy of $E_\mu = m_\mu/m_{\tilde{\tau}} \cdot E_{\tilde{\tau}}$ since $E_\mu \ll \Delta E$. On the other hand, a similar energy deposit could come for a muon with the same high energy, but the profile of the track would be significantly different, with more large energy losses along the muon track where the mul-

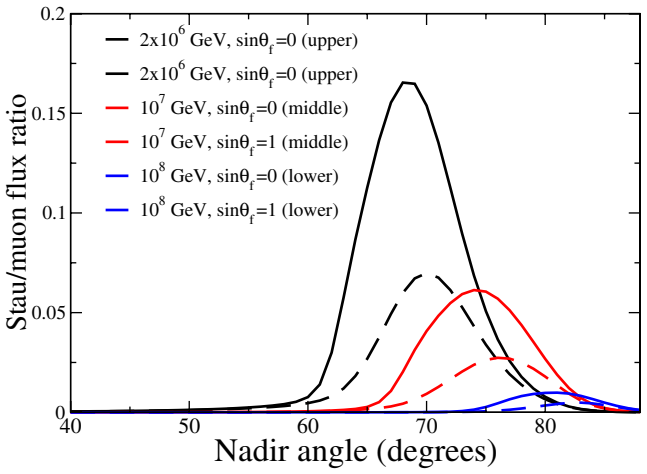

FIG. 12 (color online). The ratio of stau flux at energy rescaled by $m_{\tilde{\tau}}/m_\mu$ as a function of the nadir angle for muon energy of 10^7 GeV and 10^8 GeV including stau maximal weak interactions (dashed lines) and no weak interactions (solid lines).

tiple pair production energy losses contribute. Essential here is the large ratio of stau to muon masses. The effect is more difficult to observe when the masses are closer, e.g., for taus compared to muons [23].

In Figs. 13 and 14 we show the average number of interactions per unit distance of ice rather than the energy loss per unit distance. This is evaluated using

$$M = \frac{X\rho N_A}{A} \int_{v_{\min}}^{1} dv \frac{d\sigma}{dv}, \tag{17}$$

for density ρ and column depth X. Here we have taken $v_{\min} = \epsilon_0/E = 0.1, 0.01$ for muons and staus. The lower line on Figs. 13 and 14 are for $v_{\min} = 0.1$ and the upper lines are for $v_{\min} = 0.01$. A muon which can deposit 10% of its initial energy of 10^8 GeV proceeds to have a significantly larger number of subsequent interactions in which 10% of its energy is deposited, as compared to the stau of the same energy. The scale of the average number of interactions is such that one would need an observational coverage of a few tens of kilometer distance scales to see the distinction between muons and staus.

B. Stau showers in ice

Staus reaching the detector could interact in principle via weak interactions producing showers. Weak interactions of staus reduce its range [11], but provide an additional opportunity for its detection via interactions in ice which can provide a signal for detectors such as ANITA [12] and ARIANNA [13]. We discuss here showers produced by staus and the background due to neutrino-induced showers.

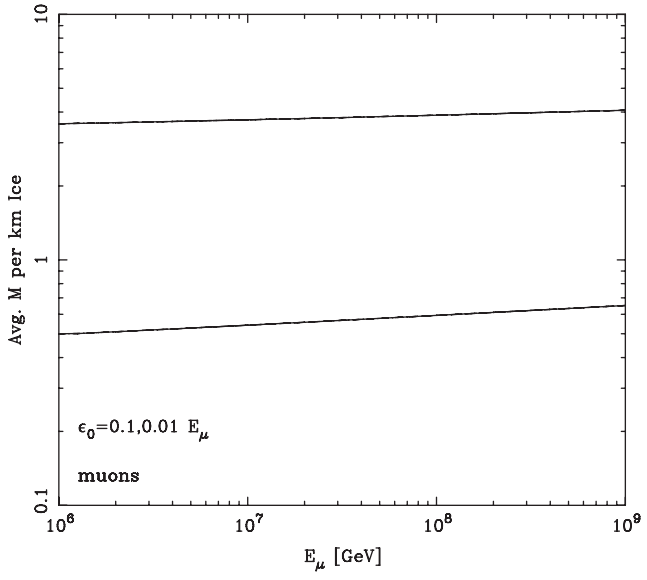

FIG. 13. The average number of interactions per km of ice for muons. The upper line is for $v > 0.01$, and the lower line is for $v > 0.1$.

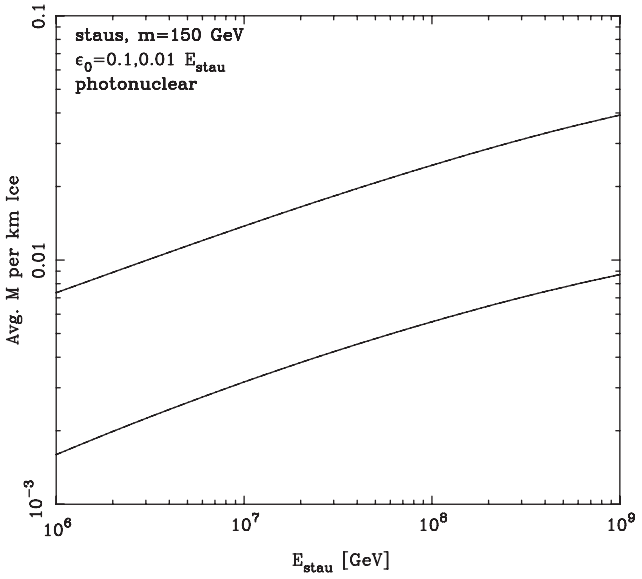

FIG. 14. The average number of interactions per km of ice for staus with $m_{\tilde{\tau}} = 150$ GeV. The upper line is for $v > 0.01$, and the lower line is for $v > 0.1$.

We have evaluated stau and neutrino showers for different nadir angles for energies above 10^6 GeV. In the shower production, we assume maximal mixing for the charged-current interactions for staus. The stau showers for a given incident angle are determined by Eq. (13), modified to include the probability to produce showers in the ice,

$$F_{\tilde{\tau},\mathrm{shr}}(E_{\mathrm{shr}}, L) = \int_0^{z_{\mathrm{ice}}} F_{\tilde{\tau}}(E_{\mathrm{shr}}, L - z') e^{-z'/\mathcal{L}^{\tilde{\tau}}_{\mathrm{CC}}} \frac{dz'}{\mathcal{L}^{\tilde{\tau}}_{\mathrm{CC}}}$$
$$\simeq F_{\tilde{\tau}}(E_{\mathrm{shr}}, L)(1 - e^{-z_{\mathrm{ice}}/\mathcal{L}^{\tilde{\tau}}_{\mathrm{CC}}}).$$

The stau interaction length due to charged-current interactions is $\mathcal{L}^{\tilde{\tau}}_{\mathrm{CC}}$. We use the interaction length for maximal weak interactions shown in Fig. 2. The path length through the ice, z_{ice}, for $\theta < 88.56°$ is given by

$$z_{\mathrm{ice}} = R_E \cos\theta - \sqrt{R_E^2 \cos^2\theta - 2R_E t + t^2}, \tag{18}$$

where R_E represents the radius of the Earth and t the average ice thickness, taken to be 2 km. For comparison, showers due to neutrinos are found from the equation,

$$F_{\nu,\mathrm{shr}}(E_{\mathrm{shr}}, L) \simeq F_{\nu}(E_{\mathrm{shr}}, L)(1 - e^{-z_{\mathrm{ice}}/\mathcal{L}^{\nu}_{CC}}). \tag{19}$$

We compare the results for the showers due to staus and neutrinos for three nadir angles: 80°, 85° and 88° in Figs. 15 and 16. All of the results in this section were obtained using the standard evolution cosmogenic flux.

In Fig. 15, the showers due to neutrinos are of the order 10^3–10^4 larger than staus at an energy of 10^6 GeV. The input neutrino flux for the stau signal will be at a higher energy than for the direct neutrino production of showers. The neutrino flux falls off as a function of energy so the

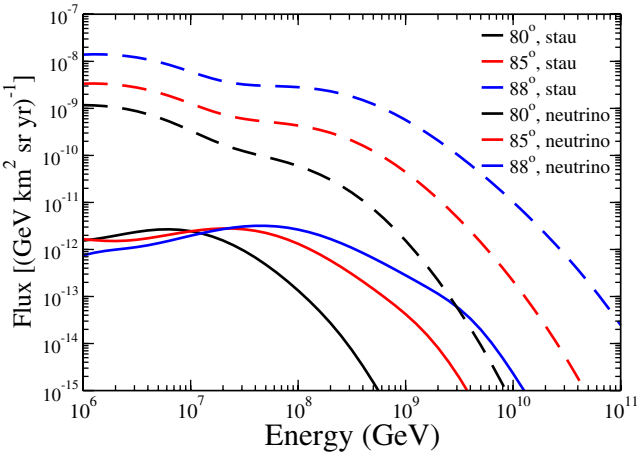

FIG. 15 (color online). The shower flux for the incident angles 80° (lower curves), 85° (middle curves), and 88° (upper curves) from staus (solid lines) and neutrinos (dashed lines).

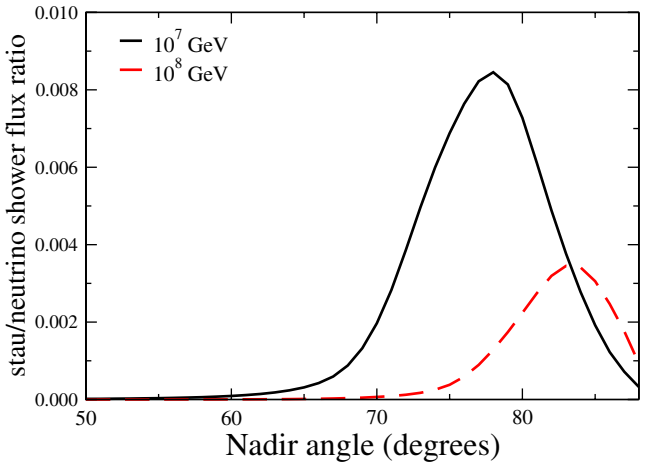

FIG. 17 (color online). The ratio of the fluxes of showers due to stau and neutrino fluxes for the energies 10^7 and 10^8 GeV as a function of incident angle.

ratio of stau to neutrino showers will be suppressed in part due to this effect. In addition, the stau flux is suppressed due to the small stau production cross section. The probability of producing showers in the detector is roughly the same for neutrinos and for staus with maximal charged-current interactions, so the inclusion of the showers is not sufficient to make up for the suppression.

The shape of the stau-induced shower flux changes relative to the neutrino-induced shower flux, so between 10^7–10^8 GeV there is a peak in the ratio of stau- to neutrino-induced showers. This effect is seen in Fig. 16, where the peak in the ratio of stau/neutrino showers appears, but as indicated, the ratio is small. It is about 0.009 for 80°.

Figure 17 shows the stau/neutrino ratio for the two fixed shower energies, 10^7 and 10^8 GeV, as a function of nadir angle. We can see that the ratio is the largest for 10^7 GeV at about 78°. The integrated flux taking into account the contribution due to all incident angles is given in Fig. 18. The maximum stau/neutrino ratio occurs for an energy of 2.5×10^7 GeV and corresponds to a stau signal only 0.33% of the neutrino signal.

Whereas muonlike signals from staus can be large compared to muon signals from neutrinos because of the long lifetime of the stau, we find that the shower signal-to-background ratio is quite small for all angles. This is due to the combination of the small production cross section for stau and the energy effects due to the chain of production and the energy loss of the stau. Stau attenuation as it traverses the Earth is roughly of the same size as neutrino attenuation, as are the probabilities for staus or neutrinos to produce showers.

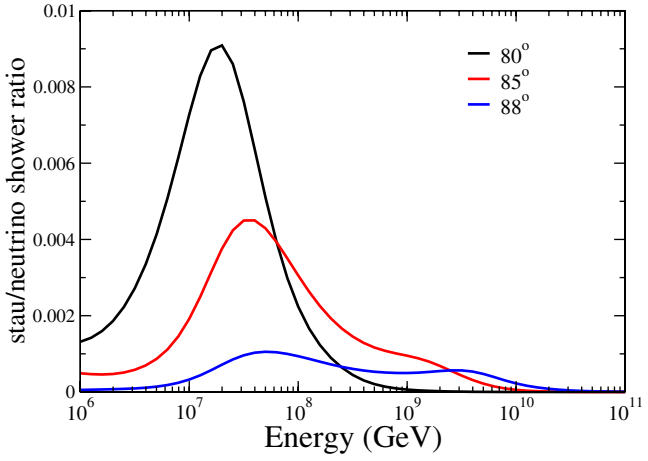

FIG. 16 (color online). The ratio of stau- to neutrino-induced shower fluxes for the incident angles 80°, 85° and 88°, represented by curves with the highest, intermediate and lowest peaks, respectively.

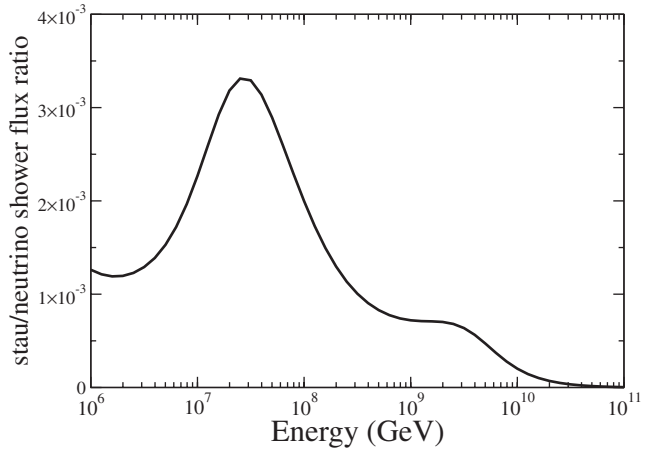

FIG. 18. The ratio of stau-induced to neutrino-induced shower fluxes, integrated over all incident angles.

V. CONCLUSIONS

We have studied signals of staus produced in interactions of cosmogenic neutrinos. We have considered two types of signals, muonlike charged tracks and showers. We have focused on low-scale supersymmetric models that have stau as NLSP, which decays into the lightest SUSY particle, the gravitino. For a sufficiently large scale of supersymmetry breaking, the stau has a very long lifetime.

Our focus has been on cosmogenic neutrino fluxes and their associated stau production in the Earth. Energy losses, both through electromagnetic and weak interactions, are important in evaluating stau signals. The energy loss of staus, however, is relatively small in comparison with muons. Thus, for some nadir angles, the stau flux is much larger than the muon flux produced in neutrino charged-current interactions.

The enhancement of the stau to muon ratio flux is larger from an input cosmogenic neutrino flux than for the Waxman-Bahcall neutrino flux [24] for energies below $E_\nu \sim 10^9$ GeV. This is mainly due to the fact that the cosmogenic flux falls less steeply than the Waxman-Bahcall flux for these neutrino energies. The neutrino flavor balance also plays a role in the stau to muon flux ratio. The large ratio of staus to muons from cosmogenic neutrinos is encouraging for experimental detection, but in order to see this signal one needs to be able to distinguish between staus and muons. Using the average energy loss per unit distance is not a good way to distinguish staus and muons, since the scaling of the energy loss parameter β has the effect of making a high-energy stau look like a lower energy muon. We have proposed a way to distinguish between stau and muon tracks by measuring the energy loss of muons via their interactions in the ice, and to use this method to reduce the background.

We also considered showers produced by staus interacting in the ice via charged-current interactions. The backgrounds for this signal are showers induced directly by neutrinos that reach the detector and interact inside the detector via charged-current or neutral-current interactions. The only way that staus would produce showers in the ice is if there is a weak mixing, but this process also contributes to reducing stau range. These effects combine with the small stau production probability to give fluxes of attenuated staus that are several orders of magnitude less than attenuated neutrino fluxes. This small stau to neutrino ratio translates directly to shower rates.

In addition to weak interactions, another possibility for shower production would be stau decays in the detector. For the parameter space considered here, with long-lived staus, the signal from decays is suppressed relative to their weak interactions.

In conclusion, stau signals at high energies are best identified by muonlike tracks. The most important detection issue is distinguishing between staus and muons, which may be possible by looking at the incremental electromagnetic energy loss as the charged particle moves through the detection volume. With very large volumes, there is a potential for detection of staus with future large neutrino telescopes.

ACKNOWLEDGMENTS

This work was supported in part by DOE Contract Nos. DE-FG02-91ER40664, DE-FG02-04ER41319 and DE-FG02-04ER41298 (Task C). We thank A. Bulmahn for discussions.

[1] See, e.g., L. Anchordoqui and F. Halzen, Ann. Phys. (N.Y.) **321**, 2660 (2006); For a review see, D. Hooper and T. Han, New J. Phys. **6**, 150 (2004); I. Sarcevic, J. Phys. Conf. Ser. **60**, 175 (2007); A. Ringwald, Nucl. Phys. B, Proc. Suppl. **136**, 111 (2004), and references therein.
[2] M. Dine, W. Fischler, and M. Srednicki, Nucl. Phys. B **B189**, 575 (1981); S. Dimopoulos and S. Raby, Nucl. Phys. **B192**, 353 (1981); L. Alvarez-Gaumé, M. Claudson, and M. B. Wise, Nucl. Phys. **B207**, 96 (1982); M. Dine and A. E. Nelson, Phys. Rev. D **48**, 1277 (1993); M. Dine, A. E. Nelson, and Y. Shirman, Phys. Rev. D **51**, 1362 (1995); M. Dine, A. E. Nelson, Y. Nir, and Y. Shirman, Phys. Rev. D **53**, 2658 (1996); For a review, see G. F. Giudice and R. Rattazzi, Phys. Rep. **322**, 419 (1999).
[3] A. Heister, *et al.*, Eur. Phys. J. C **25**, 339 (2002).
[4] J. Abdallah *et al.*, Eur. Phys. J. C **27**, 153 (2003).
[5] P. Achard *et al.*, Phys. Lett. B **517**, 75 (2001).
[6] G. Abbiendi *et al.*, Phys. Lett. B **572**, 8 (2003).
[7] I. Albuquerque, G. Burdman, and Z. Chacko, Phys. Rev. Lett. **92**, 221802 (2004); Phys. Rev. D **75**, 035006 (2007).
[8] M. Ahlers, J. Kersten, and A. Ringwald, J. Cosmol. Astropart. Phys. 07 (2006) 005; M. Ahlers, J. I. Illana, M. Masip, and D. Meloni, J. Cosmol. Astropart. Phys. 08 (2007) 008.
[9] R. Gandhi, C. Quigg, M. H. Reno, and I. Sarcevic, Astropart. Phys. **5**, 81 (1996); Phys. Rev. D **58**, 093009 (1998); M. H. Reno, Nucl. Phys. B, Proc. Suppl. **143**, 407 (2005).
[10] M. H. Reno, I. Sarcevic, and S. Su, Astropart. Phys. **24**, 107 (2005).
[11] Y. Huang, M. H. Reno, I. Sarcevic, and J. Uscinski, Phys. Rev. D **74**, 115009 (2006).
[12] S. Barwick *et al.*, Phys. Rev. Lett. **96**, 171101 (2006).
[13] S. Barwick, J. Phys. Conf. Ser. **60**, 276 (2007); A. Connolly, International ARENA Workshop on "Acoustic

and Radio EeV Neutrino Detection Activities,'' 2005, DESY Zeuthen, Germany (unpublished).
[14] R. Engel, D. Seckel, and T. Stanev, Phys. Rev. D **64**, 093010 (2001).
[15] J. Jones, I. Mocioiu, M. H. Reno, and I. Sarcevic, Phys. Rev. D **69**, 033004 (2004).
[16] O. E. Kalashev, V. A. Kuzmin, D. V. Semikoz, and G. Sigl, Phys. Rev. D **66**, 063004 (2002); **65**, 103003 (2002).
[17] S. Iyer Dutta, M. H. Reno, I. Sarcevic, and D. Seckel, Phys. Rev. D **63**, 094020 (2001).
[18] S. Eidelman *et al.* (Particle Data Group), Phys. Lett. B **592**, 1 (2004).
[19] S. I. Dutta, Y. Huang, and M. H. Reno, Phys. Rev. D **72**, 013005 (2005).
[20] R. P. Kokoulin and A. A. Petrukhin, in *Proceedings of the XII International Conference on Cosmic Rays* (Hobart, Tasmania, 1971), Vol. 6.
[21] R. P. Kokoulin and A. A. Petrukhin, Fiz. Elem. Chastits At. Yadra **21**, 774 (1990) [Sov. J. Part. Nucl. **21**, 332 (1990)].
[22] E. V. Bugaev and Y. V. Shlepin, Phys. Rev. D **67**, 034027 (2003).
[23] E. Bugaev, T. Montaruli, Y. Shlepin, and I. Sokalski, Astropart. Phys. **21**, 491 (2004).
[24] J. N. Bahcall and E. Waxman, Phys. Rev. D **64**, 023002 (2001).